Chemical mimicry of viral capsid self-assembly

Arthur J. Olson[†‡], Yunfeng H. E. Hu[†], and Ehud Keinan[†‡§]

[†]Department of Molecular Biology and the Skaggs Institute for Chemical Biology, The Scripps Research Institute, 10550 North Torrey Pines Road, La Jolla, CA 92037; and [§]Schulich Faculty of Chemistry, Technion–Israel Institute of Technology, Technion City, Haifa 32000, Israel

Communicated by Richard A. Lerner, The Scripps Research Institute, La Jolla, CA, October 7, 2007 (received for review August 15, 2007)

Stable structures of icosahedral symmetry can serve numerous functional roles, including chemical microencapsulation and delivery of drugs and biomolecules, epitope presentation to allow for an efficient immunization process, synthesis of nanoparticles of uniform size, observation of encapsulated reactive intermediates, formation of structural elements for supramolecular constructs, and molecular computing. By examining physical models of spherical virus assembly we have arrived at a general synthetic strategy for producing chemical capsids at size scales between fullerenes and spherical viruses. Such capsids can be formed by self-assembly from a class of molecules developed from a symmetric pentagonal core. By designing chemical complementarity into the five interface edges of the molecule, we can produce self-assembling stable structures of icosahedral symmetry. We considered three different binding mechanisms: hydrogen bonding, metal binding, and formation of disulfide bonds. These structures can be designed to assemble and disassemble under controlled environmental conditions. We have conducted molecular dynamics simulation on a class of corannulene-based molecules to demonstrate the characteristics of self-assembly and to aid in the design of the molecular subunits. The edge complementarities can be of diverse structure, and they need not reflect the fivefold symmetry of the molecular core. Thus, self-assembling capsids formed from coded subunits can serve as addressable nanocontainers or custom-made structural elements.

corannulene | icosahedral capsids | molecular containers | physical modeling | nanotechnology

The sphere is the simplest finite surface that partitions space. Nature uses this form at all scales in both the inanimate and living world for the basic physical property of encapsulation. Spherical virus capsids, for example, enclose space by using the geometry of the icosahedron, thus exploiting the economy of this form in terms of both surface area-to-volume ratio and genetic efficiency of subunit-based symmetric assembly (1). These capsids have 6 fivefold rotation axes, 10 threefold axes, and 15 twofold axes, providing equivalent environments for 60 identical subunits. Many virus capsids use this symmetry to create particles ranging in size from 200 to 2,000 Å. Such capsids form spontaneously from their components under the proper conditions, and they come apart under other conditions, facilitating the viral life cycle. The ubiquitous icosahedral symmetry characterizes many other natural objects, including buckminsterfullerene (C_{60}), whose small interior can accommodate single atoms or small molecules as large as a xenon atom (2).

The idea of forming nonprotein molecular containers by total synthesis and assembly of small molecules has a rich history (3–5) and is an active area of research (6–9). The field of molecular recognition is rapidly moving not only toward biomedical applications but also toward nanotechnology. Significant progress has been made in the design and synthesis of fully enclosing molecular assemblies that have inner dimensions of up to 15 Å and volumes of up to 1,500 Å^3 and are capable of encapsulating molecules that range in size from water to steroids. Many of these constructs use two molecular subunits that assemble through hydrogen bond networks or metal coordination. One of the largest molecular containers, which were formed from six calixarene subunits in cuboctahedral symmetry, could accommodate as many as eight benzene molecules (10). To the best of our knowledge, no synthetic strategy that incorporates the icosahedral symmetry of viral capsids has been reported. Although there are several reports on inorganic clusters of icosahedral symmetry (11–13), none of them mimics the function of the viral capsids as modular enclosing containers. The key component of the icosahedron is that unlike any lower-symmetry platonic solid, it contains fivefold symmetry axes. The faces of all other platonic solids are capable of a regular tiling of the plane without gaps. Thus assembly of such subunits into closed surfaces must avoid the alternative planar aggregation. In contrast, the regular pentagon cannot tile the plane, and it thus enforces curvature in its interactions with other pentagons, enclosing space with 12 pentagonal faces.

We report here a synthetic strategy that follows a cue taken from nature, using the geometric and energetic characteristics of the icosahedral viral capsids. Our design is based on self-assembly of synthetic pentagonal tiles to produce containers that have exterior diameters of 25–50 Å and interior volumes in the range of 15,000–1,000,000 Å^3.

Results and Discussion

Self-Assembly of Physical Models. *In vitro* experiments with viral capsids provide an existence proof of the feasibility of self-assembling containers that have icosahedral symmetry with 60 identical structural units (14). We decided to initially explore the generality of the phenomenon by producing autofabricated physical models of viral assembly units, choosing to model the pentameric assembly intermediate of the poliovirus (15). These structures are composed of five copies each of four individual protein chains, and they make a well shaped five-sided assembly with complementary shapes and electrostatic charges along the five edges. By appropriate placement of oriented magnets as analogs to the electrostatic complementarity, we produced a model that mimics the self-assembly of the virus from twelve pentameric assembly intermediates (Fig. 1). Placing 12 of these tiles in a container and shaking with the appropriate strength results in a stable closed shell, usually within 1–2 min [see video demonstration in supporting information (SI) Movie 1]. The key aspects of this model were the fivefold symmetric tiles, the appropriate curvature at the tile interfaces, and the geometric and magnetic complementarity of the interfaces. Although intellectually we knew that this type of self-organization occurs spontaneously, watching it happen from random shaking on the macroscopic scale was inspirational.

One question that arises from this physical experiment is as follows: Given the number of interfaces that need to form, why does this assembly take place so rapidly? Clearly the answer is in the symmetries of the tiles and capsid and the redundancy of the interfaces; they are all self-complementary and there are five

Author contributions: A.J.O. and E.K. designed research; A.J.O., Y.H.E.H., and E.K. performed research; A.J.O., Y.H.E.H., and E.K. analyzed data; and A.J.O. and E.K. wrote the paper.

The authors declare no conflict of interest.

Freely available online through the PNAS open access option.

[‡]To whom correspondence may be addressed. E-mail: olson@scripps.edu or keinan@tx.technion.ac.il.

This article contains supporting information online at www.pnas.org/cgi/content/full/0709489104/DC1.

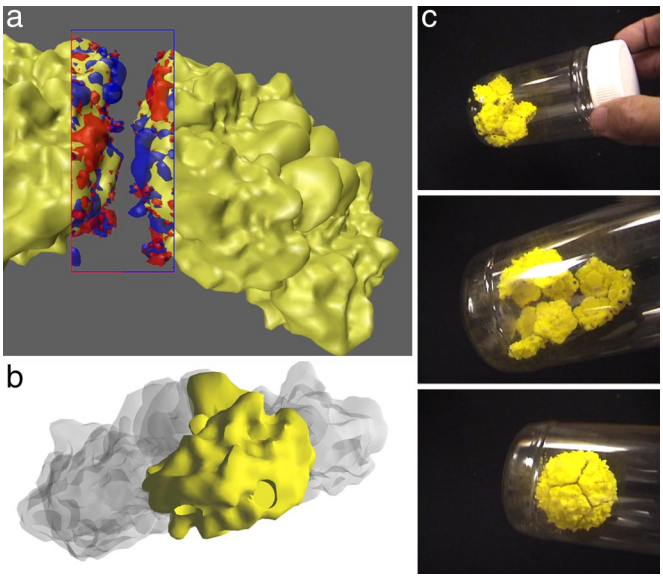

Fig. 1. From molecular structure to self-assembling plastic model. (*a*) Two poliovirus pentameric assembly intermediates, showing the electrostatic complementarity of the interface between them (red negative, blue positive electrostatic contours). (*b*) Geometry used to make the autofabricated pentameric tile. (*c*) Sequence showing self-assembly by shaking of the 12 tiles into a complete capsid.

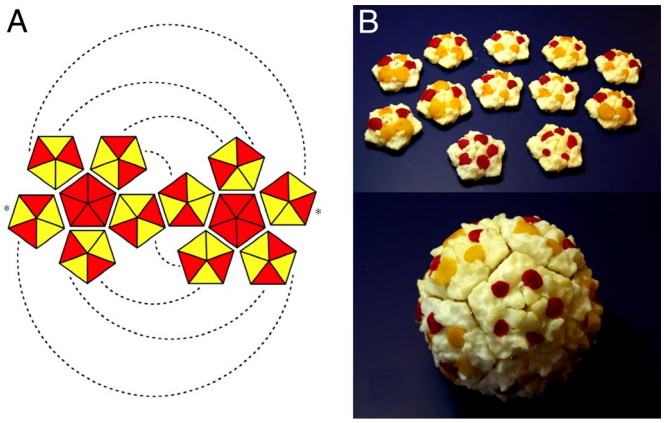

Fig. 2. Assembly of coded tiles. (*A*) Combinatorial scheme with two tile types and two edge types (the dashed lines and asterisks indicate pairs of interacting edges). (*B*) Assembled tiles in the only possible configuration with red tiles at poles.

equivalent faces per tile, and there is only one most stable configuration, the assembled capsid. The number of ways that a dodecahedron can be put together from 12 identical pentagonal tiles is $11! \times 5^{12} = 9.75 \times 10^{15}$. Thus, the degeneracy of the interactions allows a very large number of physical interactions to lead to productive interface formation for an intact capsid.

An interesting version of this experiment would be the spontaneous resolution of homochiral capsids. One might imagine what would happen if there were two different types of tiles each with self-complementary edges, but incompatible with the other type, for example enantiomeric pentagons. Clearly, mixing these two types of tiles would result in self-assembly of two different types of capsids, each made of only one of the tile types. To test this physically, we built two types of poliovirus capsid tiles (colored red and green), with the magnet pairs on each face of the red type reversed compared with the green type. Shaking up a container with 12 red and 12 green tiles results in two intact spheres each containing tiles of only one color. The assembly in this experiment takes significantly longer, but usually <10 min (see video demonstration in SI Movie 2).

Design of Programmed Assembly of Coded Tiles. Because there are numerous ways to construct complementarity, using distribution of polar elements, one can easily design tiles with different patterns of polarity on each edge of the pentagon, each with a distinct complementary edge mate. If the interface formed by any complementary pair is isostructural with all others, then any combination of 12 tiles with appropriately matched edges can form a complete, stable dodecahedral structure. This fact opens up the possibility of creating self-assembling systems that produce a large diversity of patterned capsids.

To illustrate this possibility we designed a system using non-self-complementary interfaces formed from opposite polarity (red and yellow). We created two tile types (all-red and mixed). The all-red tile had five identical edges, whereas the mixed was composed of two red and three yellow edges (Fig. 2 *A* and *B*). It is easy to demonstrate that a dodecahedron built from these two tile types can assemble only with 2 red tiles and 10 mixed tiles because any other combination would have an unequal number of red and yellow edges. Moreover, the red tiles can occupy only special positions on the dodecahedron: they must be at opposite poles (with two pentagons separating them), because any closer placement of the all-red tiles (touching or one pentagon removed) is not possible with all edges complementary. The mixed tiles themselves must orient in a specific way around each pole, with each half-dodecahedron (or hemisphere) exhibiting "color-mirror" symmetry.

Our autofabricated poliovirus tiles and different magnet placement could be used to test this idea in a physical situation. The all-red tile type was constructed with both magnets on each edge facing in the same direction. The mixed tile type (yellow–red) had the pattern of polarities described above, with two edges as in the red tile and three of opposite polarity. Shaking up 12 or more of these tiles, whether in stoichiometric proportions (2 to 10) or not, should result in the expected assembly of only capsids with two red tiles at opposite ends of the capsid. However, to estimate the relative time for assembly, we needed to calculate how many ways this configuration of tiles could form an intact capsid. The red tiles can go in $2! \times 5^2 = 50$ ways, and the mixed tiles can go in $10! \times 2 =$ 7,257,600 ways. Assuming that the relative amount of assembly redundancy is a good estimate of the time to assemble, an intact capsid of a poliovirus capsid composed of these two tile types would take $9.75 \times 10^{15}/(50 \times 7.26 \times 10^6) = 2.7 \times 10^7$ times longer to form. Given that the assembly time using only one type of uniform tile is ≈1 min, we would expect this shaking experiment to take ≈50 years.

The physical demonstration of tile self-assembly showed that a mechanism used by viral capsids could apply to the macroscopic scale. The experiments using different tile types in combination showed that such self-assembly could go beyond homogeneous assemblies to create diverse patterned closed containers, but at a much less efficient rate. However, if the tiles were of a small enough scale, so that we were dealing with very large numbers interacting at very rapid speeds, such combinatorics would be feasible on a reasonable time scale. This reasoning has led us to examine the possibility of translating these tile designs back into molecular structures that can be chemically synthesized.

Design of Synthetic Molecular Pentagonal Tiles. Our physical demonstrations of viral assembly on the macroscopic scale inspired us to examine the same principles on the scale accessible to synthetic chemistry. Overall, the general problem of synthetic capsids can be solved by the chemical synthesis of pentagonal tiles with appropriate "sticky" edges and by finding the appropriate conditions for their self-assembly. Aiming at the total synthesis of such pentagonal

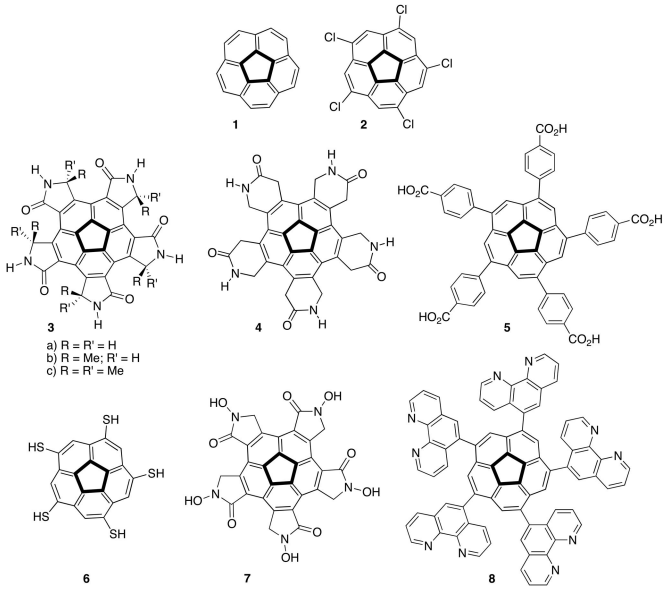

Fig. 3. Corannulene and derived chemical structures.

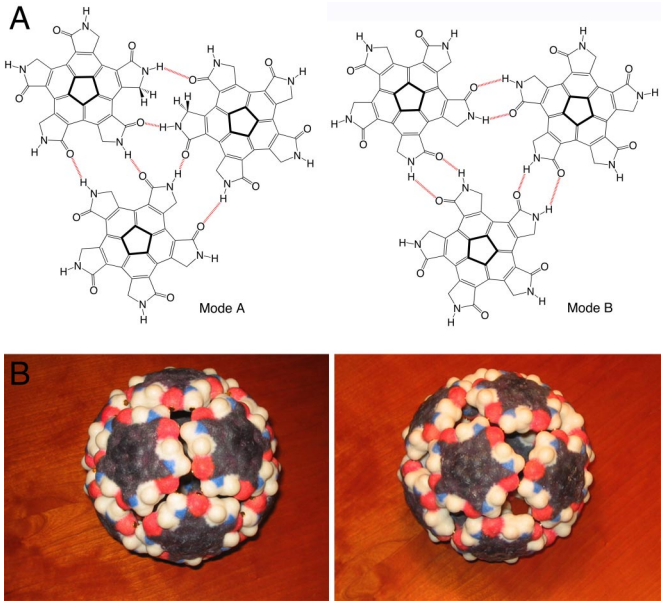

Fig. 4. Self-assembly of 12 corannulene-derived tiles to form a chemical capsid by hydrogen bonding. (*A*) Two modes of possible self-assembly of the pentagonal tile **3a**, shown from the threefold axis of the icosahedron. (*B*) Self-assembly of the model tiles showing mode A (*Left*) and mode B (*Right*).

tiles, we searched for structural cores that have a fivefold symmetry, appropriate curvature, and rigidity. We have chosen the corannulene skeleton (**1**, $C_{20}H_{10}$; Fig. 3), nicknamed "buckybowl," which has a rigid fivefold-symmetric scaffold with suitable curvature (16). The pentagonal ring in corannulene is surrounded by six aromatic rings, thus creating a bowl whose depth is defined as the distance between the plane of the five-membered ring (core) and ten peripheral carbon atoms (rim). Because the synthesis of **1** is now well established, the first synthesis being published four decades ago (17), the synthetic challenge for self-assembly involves mainly the attachment of a binding device to each of its five corannulene edges.

The well developed synthetic methodology for corannulene substitution and for unidirectional substitution patterns, in particular, allows for the synthesis of various pentagonal tiles (16). For example, the systematic conversion of **1** into a variety of *sym*-pentasubstituted corannulene derivatives can lead to the appropriate placement of the desired functional groups around the rim of the bowl with fivefold symmetry (18–20). A convenient entry to such compounds is *sym*-pentachlorocorannulene, **2**, which is obtained by chlorination of **1** with iodine monochloride (21, 22). The various examples of potential tiles illustrated in Fig. 3 are all based on four design elements: (*i*) fivefold symmetry, (*ii*) capsid thermodynamic stability, (*iii*) capsid kinetic instability, and (*iv*) built-in mechanism for capsid disassembly. The latter element is needed to allow disintegration of the chemical capsid to enable loading and unloading of the desired cargo in its interior.

The requirement for kinetic instability is a crucial design element (23). The self-assembly of 12 pentagonal tiles to form an icosahedral chemical capsid represents the arrival at the global free energy minimum of the system. Achieving this minimum is not trivial because tiles can assemble and aggregate in many alternative ways to produce off-pathway products that are less thermodynamically stable than the intact capsid but kinetically stable. For example, various aggregates that represent local minima but are insoluble in the medium could irreversibly precipitate out of the solution. Therefore, to allow the system to reach the desired global minimum it is important that the self-assembly of the tiles is maintained under conditions of uninterrupted equilibrium. Thus, reversibility is essential to allow for self-correction during the self-assembly process. To achieve both thermodynamic stability and kinetic instability it is essential that any formation of aggregates would be fast and reversible and that all aggregates would be soluble.

The examples in Fig. 3 represent solutions to this problem by using functional groups that can self-assemble by means of hydrogen bonding, including carboxylic acids and amides, such as **3**–**5**. The main advantage in using such functional groups is the opportunity to quickly arrive at the global minimum of the system by fast exchange of hydrogen bonds. The synthesis of all derivatives can employ **2** as a key intermediate. Simple molecular modeling predicts that the γ-lactam derivative, **3a**, would be more rigid than the δ-lactam analog, **4**, and therefore more appropriate to produce the desired chemical capsid. Yet, the slight flexibility of **4** could allow for optimal spatial adjustment of the relative positioning of these tiles. The pentacarboxylic acid, **5**, is even more flexible as a result of the free rotation around two single bonds in each of the five side chains.

In principle, the acceptor–donor pair presented on each pentagonal edge of the hydrogen-bonded tiles, **3**–**5**, could allow for two different binding modes (Fig. 4). In mode A each amide group is bound to two other amide groups that are positioned on two neighboring tiles. In contrast, in mode B each amide group is bound to a single amide function of a neighboring molecule. At first glance it is difficult to assess which mode would prevail in solution. Nevertheless, the mode of binding would have significant consequences on the potential applications of the resultant capsids. Whereas mode A would produce tightly closed capsids that do not allow even the exchange of water molecules between the interior and exterior, mode B would lead to a slightly bigger capsid that has sufficiently large holes, located at the threefold axes, that allow free exchange of water and even larger molecules.

The construction of synthetic capsids by using self-assembly of **3a** by mode A produces a particle with an outside diameter of ≈25 Å, which places it in a scale between a buckyball (≈9 Å) and the small virus capsid of satellite tobacco necrosis virus (≈150 Å) (Fig. 5). One can envision the construction of larger capsids by using pentagonal tiles having much longer side chains.

Molecular Modeling of Chemical Capsid Assembly. For the past four decades corannulene has intrigued not only synthetic chemists but also theoreticians, who focused mainly on the bowl-to-bowl inversion (24–26) and the substitution effect on the bowl depth. We have

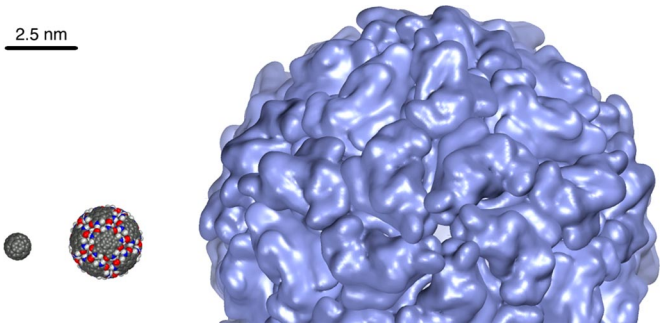

Fig. 5. Same-scale comparison of C_{60} (left), chemical capsid **3** mode A (center), and satellite tobacco necrosis virus (right), each viewed along a fivefold symmetry axis.

used computational molecular modeling to investigate the propensity of the lactam derivatives in series **3** to self-assemble to a spherical dodecameric chemical capsid. The results of this modeling study could be very helpful for the design and synthesis of the appropriate pentagonal tiles of such capsids. Our main concern was the competition between two self-assembly processes, either edge-to-edge binding through intermolecular hydrogen bonding or van der Waals stacking.

Recently, density functional theory at B3LYP/6-31G* was shown to best reproduce the x-ray-derived corannulene geometry (27). We therefore chose to use B3LYP/6-31G* in Gaussian 03 (28) to optimize geometries in all series **3** monomer and dimer structures. Frequencies were also computed to obtain zero-point energy-corrected free energies. For molecular dynamics simulations we constructed a $5 \times 5 \times 5$ cubic grid with cell edges equal to the longest two-point distance within a molecule (12.8 Å, Fig. 6). We then placed a copy of the molecule at the center of each of the 125 cells and assigned each a random molecular orientation. This array was placed in a larger box (80 Å on a side) that was solvated with water or acetonitrile by using periodic boundary conditions. In this box there were 125 molecules of **3** and 3,177 solvent molecules, with the concentration of **3** being 0.8 M.

Charges of **3** used in MD were calculated by Gaussian 03 with keywords [#HF/6-31G* opt SCF=tight Test Pop=mk iop(6/33 = 2) iop(6/42 = 6)]. Force field parameters were generated with the antechamber module in Amber 9 (29). The explicit solvent box was added by xleap with periodic boundary conditions. SHAKE was added on bonds involving hydrogen atoms. The time step was set to 2 fs. Langevin dynamics was used with a collision frequency of 1.0 ps^{-1}. Initially, a weak restraint was added to the solvent molecules and then the entire system was heated to 300 K and equilibrated for 200 ps. Data were then collected from a 5.2-ns MD simulation for **3b**.

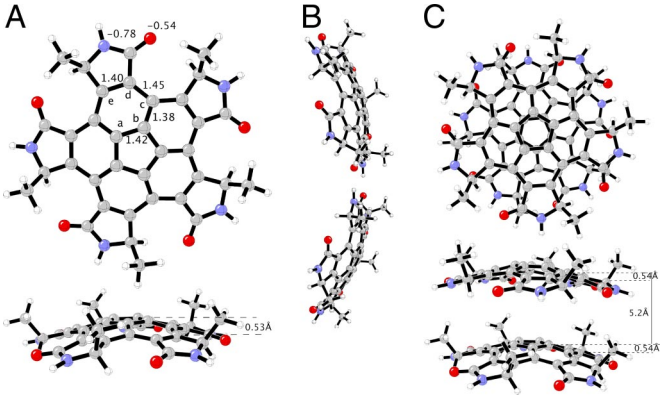

Fig. 6. Optimized geometries of **3b** with CHELPG (charges from electrostatic potentials using a grid-based method) charges (*A*), edge-to-edge dimer (*B*), and stacked dimer with B3LYP/6-31G* (*C*).

The quantum mechanical optimized geometry of **3b** shows that the hub, spoke, flank, and rim lengths (Fig. 6*A*) are 1.42 (ab), 1.38 (bc), 1.45 (cd), and 1.40 (de) Å, respectively, which are identical to the distances reported in the x-ray crystal structures of corannulene (27) except that the rim (de) in **3b** is slightly longer than in corannulene (1.38 Å), probably because of the angle constraint from the fused lactam ring. Among all four types of corannulene carbon–carbon bonds, the flank (cd) has the least double bond character. The depth of the **3b** bowl is 0.53 Å, which is significantly smaller than corannulene (0.88 Å) and also indicates a low bowl-to-bowl conversion barrier (24, 30). A pair of symmetrical N–H···O hydrogen bonds at 2.9 Å connect two **3b** molecules to form an edge-to-edge dimer (Fig. 6*B*). The charges on both nitrogen and oxygen atoms are slightly more negative at −0.82 and −0.58 in comparison to −0.78 and −0.54 in the isolated **3b**, respectively (Fig. 6*A*). The quantum mechanical computed enthalpy of edge-to-edge dimer formation is −15.8 kcal/mol. Fig. 6*C* shows a stacked dimer with different views. Two **3b** molecules are in an eclipsed-like conformation to each other and N(–H) and O(=C) groups are on top of each other, which not only achieves more van der Waals contact between two corannulene rings but also enhances the favorable dipole–dipole interactions. In the **3b** dimer the distance between the overlapped N(–H) and O(=C) atoms is 5.2 Å, whereas it is 3.4 Å in the stacked **3a** dimer, due primarily to steric interactions of the methyl groups at the rim. Nevertheless the two molecules in both the edge-to-edge and stacked **3b** dimer have uniform geometry nearly identical to the isolated monomeric form (Fig. 6*A*).

Table 1 shows the energetics from a set of isolated molecular dynamics (MD) simulations of the key intermediate states in **3a** and **3b** self-assembly. To assess the energetics and stability of these structures MD simulations were performed in vacuum for both stacked and hydrogen-bonded configurations. For the hydrogen-bonded oligomers, both the more compact mode A and the more open mode B (Fig. 4*A*) were evaluated. According to these *in vacuo* molecular dynamics studies, most of edge-interacting dimers, trimers, and tetramers are not stable at room temperature and quickly disassemble into various stacked configurations. However, we have shown (see SI Fig. 9) that the sum of van der Waals and electrostatic energies is temperature independent, which allowed us to carry out the simulations at lower temperatures (100 K). We found for **3a** that the mode B spherical dodecamer is 35 kcal/mol more stable than the sphere of mode A. However the corresponding stacked oligomers of **3a** are always more stable than the edge-to-edge oligomers at any level of assembly. This observation originates from the significant increase of the van der Waals interactions upon stacking, whereas there is very little change in the electrostatic interactions.

The strong van der Waals complementary between a stacked pair of **3a** subunits outweighs the energy gains from the formation of intermolecular hydrogen bonds in either mode A or mode B for **3a**. Therefore we designed the **3b** structure to disrupt the van der Waals interactions between stacked dimers and also to potentially increase the polarity and thus the strength of the intermolecular hydrogen bonds. As expected, the stacking energy is reduced from 39 kcal/mol to 32 kcal/mol, whereas the edge interaction is increased from 7 kcal/mol to 18 kcal/mol in the **3b** dimer interaction, mainly because of the enhanced strength of the hydrogen bonds (Table 1). The intact spherical dodecamer of **3b** was found to be more stable than a stacked dodecamer by 86 kcal/mol.

To more strongly promote intermolecular hydrogen bond formation we used acetonitrile as the solvent instead of water. In explicit acetonitrile solvent, no **3a** hydrogen bonded trimers or higher oligomers were observed after 2.5 ns. At most only isolated dimers were formed and remained throughout the simulations. In contrast with **3b**, after a 5-ns MD simulation in acetonitrile, a

Table 1. Energetics (kcal/mol) of formation of various 3a and 3b oligomers from 2-ns molecular dynamics in vacuum

	E_{vdw}	ΔE_{vdw}	E_{ele}	ΔE_{ele}	$E_{vdw} + E_{ele}$	$\Delta E_{vdw} + \Delta E_{ele}$
			Monomer			
3a	6 ± 3		−310 ± 4		−304	
3b	7 ± 4		−646 ± 8		−639	
	Dimer. No. of edge interfaces = 1; stacked interfaces = 1					
3a B	11 ± 2	−1	−626 ± 4	−6	−615	−7
3a A	9 ± 2	−3	−624 ± 4	−4	−615	−7
3a S	−29 ± 4	−41	−618 ± 6	2	−647	−39
3b B	9 ± 3	−5	−1,305 ± 7	−13	−1,296	−18
3b S	−16 ± 6	−30	−1,294 ± 12	−2	−1,310	−32
	Trimer. No. of edge interfaces = 3; stacked interfaces = 2					
3a B	16 ± 6	−2	−958 ± 9	−28	−942	−30
3a A	12 ± 6	−6	−950 ± 9	−20	−938	−26
3a S	−66 ± 5	−84	−928 ± 7	2	−994	−82
3b B	12 ± 4	−9	−1,981 ± 8	−43	−1,969	−52
3b S	−40 ± 7	−61	−1,943 ± 15	−5	−1,983	−66
	Tetramer. No. of edge interfaces = 5; stacked interfaces = 3					
3a B	21 ± 7	−3	−1,292 ± 10	−52	−1,271	−55
3a A	15 ± 7	−9	−1,278 ± 10	−38	−1,263	−47
3a S	−104 ± 6	−128	−1,239 ± 8	1	−1,343	−127
3b B	18 ± 8	−10	−2,652 ± 17	−68	−2,634	−78
3b S	−64 ± 9	−92	−2,593 ± 10	−9	−2,657	−101
	Hexamer. No. of edge interfaces = 10; stacked interfaces = 5					
3a B	30 ± 9	−6	−1,973 ± 13	−113	−1,943	−119
3a A	18 ± 8	−18	−1,948 ± 13	−88	−1,930	−106
3a S	−181 ± 8	−217	−1,861 ± 10	−1	−2,042	−218
3b B	24 ± 10	−18	−4,014 ± 21	−138	−3,990	−156
3b S	−112 ± 11	−154	−3,892 ± 23	−16	−4,004	−170
	Dodecamer. No. of edge interfaces = 30; stacked interfaces = 11					
3a B	55 ± 14	−17	−4,087 ± 20	−367	−4,032	−384
3a A	21 ± 13	−51	−4,018 ± 20	−298	−3,997	−349
3a S	−410 ± 11	−482	−3,727 ± 15	−7	−4,137	−489
3b B	35 ± 15	−49	−8,171 ± 31	−419	−8,136	−468
3b S	−257 ± 16	−341	−7,793 ± 34	−41	−8,050	−382

E_{vdw}, van der Waals energy; E_{ele}, electrostatic energy; multimer interactions A, B, and S, edge mode A, B, and stacked, respectively.

half-sphere hexamer was observed along with several edge-to-edge trimers, tetramers, and pentamers. The snapshots of trimer, tetramer, pentamer, and half-sphere are taken at 600 ps, 1.7 ns, 4.1 ns, and 4.9 ns, respectively (Fig. 7). During the assembly of the half-sphere, the fourth **3b** molecule to join the trimer structure spends most of its time with one N–H···O hydrogen bond connected to the trimer until it orients appropriately to form a second O···H–N hydrogen bond and a pair of extra hydrogen bonds with the neighbor **3b** to complete the formation of a tetramer. It takes longer time (>2 ns) for a fifth **3b** molecule to drag itself and another **3b** molecule associated in a dimer toward the tetramer. Similarly, the last **3b** molecule in the half-sphere quickly attaches itself to the dome once the first pair of hydrogen bonds is created. Two more **3b** molecules are added to the half-sphere structure during the following 5-ns MD simulations (data not shown).

In the MD simulation, few oligomers appear to dissociate once formed. Fig. 8 shows the formation of various oligomers as time progresses. An almost instantaneous increase of dimer (yellow) content accompanied by the drop of monomer (green) is seen at the very beginning of the simulation. The formation of trimer (cyan), tetramer (blue), and pentamer (pink) has plateaued at ≈1 ns, 2.5 ns, and 4.2 ns, respectively. At the end of 5.2 ns of simulation, one half-sphere structure (red) was formed (see video demonstration in SI Movie 3).

Two other MD grids of **3b** were examined with one-third and one-eighth the solute concentration of the original simulation. With the same MD protocol, more stacked dimers were observed in comparison with the simulation with the original **3b** concentration

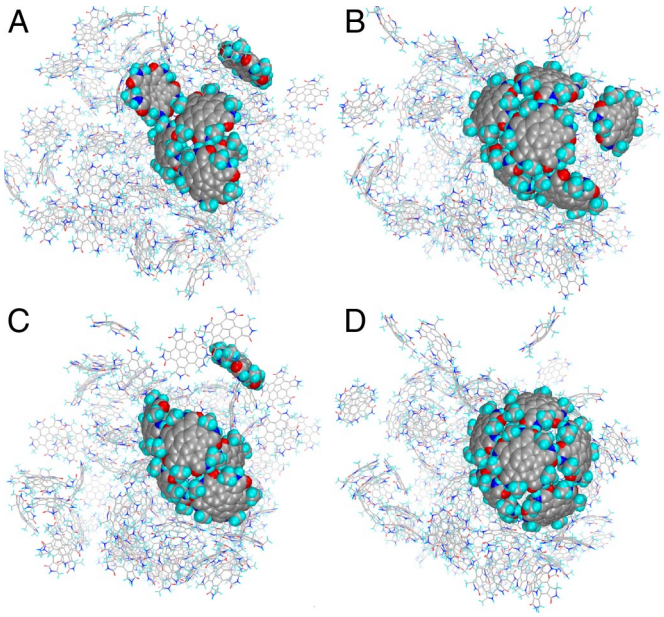

Fig. 7. Four snapshots from molecular dynamics simulations with explicit acetonitrile solvent and periodic boundary conditions. (*A*) Trimer (at 600 ps). (*B*) Tetramer (at 1.7 ns). (*C*) Pentamer (at 4.1 ns). (*D*) Half-sphere hexamer (at 4.9 ns). The same six **3b** molecules of the final half-sphere structure are shown as CPK (Corey–Pauling–Koltun) models in all snapshots, and the other molecules in the simulation are represented as lines. Solvent molecules are not shown.

at the same period of simulation time. More trimers were generated in the simulation at the higher concentration than at the lower.

From the vacuum MD simulations we observe that **3a** molecules tend to form various stacked dimers easily and do not undergo edge-to-edge assembly as efficiently as **3b** molecules do under the same conditions. Both **3a** and **3b** arrays quickly disintegrate into various stacked oligomers in vacuum because of the rugged potential surface and local entrapment of the stacked oligomers. The polar solvent acetonitrile can easily solvate **3b** molecules without compromising their potential to form intermolecular hydrogen bonds. This solvent can also act as a buffer to slow down the stacking process. In fact, the use of aromatic solvents could discourage stacking and favor the desired edge-to-edge hydrogen-bonding

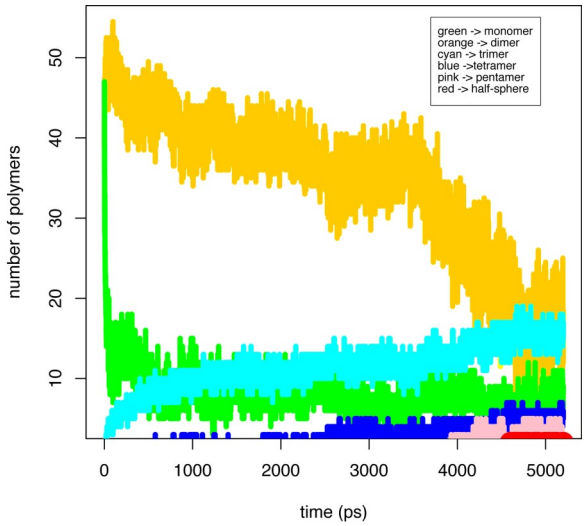

Fig. 8. The compositional variation of the 5 × 5 × 5 **3b** lattice in a 5.4-ns MD simulation. Linewidth of the half-sphere band is increased for viewing purposes.

interaction. A lattice with higher **3b** density provides increased opportunity for successful hydrogen-bonding interactions among neighboring molecules over the less favorable stacking. The key is therefore to design molecules and solvent systems that disrupt stacking while allowing rapid hydrogen-bond formation along the desired assembly pathway.

Other Opportunities of Capsid Design. Dynamic covalent chemistry offers attractive opportunities of doing supramolecular chemistry at the level of covalent bonds (23). Of particular interest is the possibility of forming stable chemical capsids by using disulfide bonds as the binding device. Whereas the disulfide bond is kinetically stable at low pH (<5), disulfide exchange occurs rapidly at moderate to high pH (31, 32). The exchange may even be performed in water, thus providing access to many biomimetic systems. For example, a collection of dithiol building blocks have been used to generate dynamic combinatorial libraries of macrocyclic disulfides (33). This approach can produce a covalently assembled capsid by thiolate anion-catalyzed exchange of the disulfide bonds in *sym*-penta(phenyldisulfido)chlorocorannulene that is derived from pentamercaptocorannulene, **6** (Fig. 3). Other attractive dynamic covalent systems involve transacetalization that goes via transesterification under basic conditions, formal metathesis under acidic conditions (34), and imine formation/exchange (35–37).

Metal coordination and metal-directed self-assembly represent attractive, well proven strategies for the design of large multicomponent cage assemblies (38, 39). Interestingly, in the case of coordination capsules assembled from 6-pyrogallol[4]arene the capsule assembled with Cu(II) ions is structurally analogous to its hydrogen-bonded counterpart (40). The use of coordination chemistry offers a plethora of assembly as well as disassembly opportunities. A corannulene unit that is armed with a polydentate ligand at each of its edges cannot self-assemble alone but can form very strong assemblies in the presence of the appropriate metal ions. Although corannulene itself can coordinate to transition metals, this type of coordination cannot result in closed containers (41). Several appropriate tiles of this family could be based on the binding properties of hydroxamic acid, such as **7** (Fig. 3), phenanthroline, such as **8**, trispyrazolylborate, dithiocarbamate, etc. The appropriate choice of metals and ligands can offer very high binding constants, up to the equivalent of a covalent bond and yet, under appropriate conditions, these chemical capsids would disintegrate back to the individual tiles. For example, the metal complexes can dissociate as a result of depletion of the metal ions from the medium, change of pH, of change of the metal oxidation state.

Conclusions

We have demonstrated with physical models that self-assembly of intact dodecahedral capsids from individual components can be accomplished at a wide variety of scales. Such assembly can take place by designing complementary edges on pentagonal tiles. Chiral tiles can be spontaneously resolved into homochiral capsids, and coded tiles with variation of edge complementarity can produce a wide variety of distinct capsid types.

We have translated these models to the molecular scale by using the pentagonal core of corannulene, making possible the chemical synthesis of spherical containers on a scale between fullerenes and viral capsids. Such structures can serve numerous functional roles, including chemical microencapsulation and delivery of drugs and biomolecules, epitope presentation to allow for a new platform for immunization, observation of encapsulated reactive intermediates (42), synthesis of nanoparticles of uniform size, and as structural elements for supramolecular constructs.

Our computational models based upon optimized quantum mechanical geometries and molecular dynamics simulations indicate that appropriately designed corannulene derivatives can self-assemble. We have tested a self-assembly process making use of intermolecular hydrogen bonds and molecular shape complementarity among pentalactamocorannulene molecules. Molecular dynamics of 125 **3b** molecules in explicit acetonitrile solvent shows the rapid formation of a half-sphere hexameric structure. Ultimately, longer simulation should lead to the intact dodecahedral structure. The present study gives us confidence that we can design molecules based upon these principles that can assemble into chemical capsids.

ACKNOWLEDGMENTS. A.J.O. thanks Jon Huntoon for assistance preparing the physical models. Y.H.E.H. thanks Dr. Qing Zhang for helpful discussions. The tangible model research and development was supported by National Institutes of Health Grant R33EB00798 and National Science Foundation Grant EIA0121282 to A.J.O. and by and National Science Foundation Grant 0523928 to E.K. This study was also supported by the Israel Science Foundation, the German–Israeli Project Cooperation (DIP), the Institute of Catalysis Science and Technology, Technion, and The Skaggs Institute for Chemical Biology. E.K. is the incumbent of the Benno Gitter and Ilana Ben-Ami Chair of Biotechnology, Technion. A.J.O. was an Institute of Advanced Study Distinguished Fellow at Durham University during the completion of the manuscript.

1. Crick FHC, Watson JD (1956) *Nature* 177:473–475.
2. Saunders M, Jimenez-Vazquez HA, Cross RJ, Mroczkowski S, Gross ML, Giblin DE, Poreda RJ (1994) *J Am Chem Soc* 116:2193–2194.
3. Cram DJ (1988) *Angew Chem Int Ed Engl* 27:1009–1020.
4. Lehn J-M (1988) *Angew Chem Int Ed Engl* 27:90–112.
5. Pedersen CJ (1988) *Angew Chem Int Ed Engl* 27:1021–1027.
6. Rudkevich DM (2002) *Bull Chem Soc Jpn* 75:393–413.
7. Hof F, Craig SL, Nuckolls C, Rebek J, Jr (2002) *Angew Chem Int Ed* 41:1488–1508.
8. Turner DR, Pastor A, Alajarin M, Steed JW (2004) *Struct Bonding* 108:97–168.
9. Dalgarno SJ, Atwood JL, Raston CL (2006) *Chem Commun* 44:4567–4574.
10. Rebek J, Jr (2005) *Angew Chem Int Ed* 44:2068–2078.
11. Alvarez S (2005) *Dalton Trans* 2209–2233.
12. Müller A, Sarkar S, Shah SQN, Bogge H, Schmidtmann M, Sarkar S, Kogerler P, Hauptfleisch B, Trautwein AX, Schunemann V (1999) *Angew Chem Int Ed* 38:3238–3241.
13. McKinlay RM, Dalgarno SJ, Nichols PJ, Papadopoulos S, Atwood JL, Raston CL (2007) *Chem Commun* 2393–2395.
14. Harrison S (2001) *Curr Opin Struct Biol* 11:195–199.
15. Hogle JM, Chow M, Filman DJ (1985) *Science* 229:1358–1365.
16. Wu Y-T, Siegel JS (2006) *Chem Rev* 106:4843–4867.
17. Barth WE, Lawton RG (1966) *J Am Chem Soc* 88:380–381.
18. Sygula A, Xu G, Marcinow Z, Rabideau PW (2001) *Tetrahedron* 57:3637–3644.
19. Bancu M, Rai AK, Cheng P, Gilardi RD, Scott LT (2004) *Synlett* 173–176.
20. Grube GH, Elliot EE, Steffens RJ, Jones CS, Baldridge KK, Siegel JS (2003) *Org Lett* 5:713–716.
21. Seiders TJ, Elliott E, Grube G, Siegel JS (1999) *J Am Chem Soc* 121:7804–7813.
22. Scott LT (1996) *Pure Appl Chem* 68:291–300.
23. Rowan SJ, Cantrill SJ, Cousins GRL, Sanders JKM, Stoddart JF (2002) *Angew Chem Int Ed* 41:898–952.
24. Biedermann PU, Pogodin S, Agranat I (1999) *J Org Chem* 64:3655–3662.
25. Samdal S, Hedberg L, Hedberg K, Richardson AD, Bancu N, Scott LT (2003) *J Phys Chem A* 107:411–417.
26. Seiders TJ, Baldridge KK, Grube GH, Siegel JS (2001) *J Am Chem Soc* 123:517–525.
27. Petrukhina MA, Andreini KW, Mack J, Scott LT (2005) *J Org Chem* 70:5713–5716.
28. Frisch MJ, Trucks GW, Schlegel HB, Scuseria GE, Robb MA, Cheeseman JR, Montgomery JA, Jr, Vreven T, Kudin KN, Burant JC, *et al*. (2003) Gaussian 03 (Gaussian, Pittsburgh), Revision B.05.
29. Case DA, Darden TA, Cheatham TE, III, Simmerling CL, Wang J, Duke RE, Luo R, Merz KM, Wang B, Pearlman DA, Crowley M, *et al*. (2006) AMBER 9 (Univ. California, San Francisco).
30. Dinadayalane TC, Deepa S, Reddy AS, Sastry GN (2004) *J Org Chem* 69:8111–8114.
31. Furusho Y, Hasegawa T, Tsuboi A, Kihara N, Takata T (2000) *Chem Lett*, 18–19.
32. Shimizu T, Murakami H, Kobayashi Y, Iwata K, Kamigata N (1998) *J Org Chem* 63:8192–8199.
33. Otto S, Furlan RLE, Sanders JKM (2000) *J Am Chem Soc* 122:12063–12064.
34. Cacciapaglia R, Di Stefano S, Mandolini L (2005) *J Am Chem Soc* 127:13666–13671.
35. Cantrill SJ, Rowan SJ, Stoddart JF (1999) *Org Lett* 1:1363–1366.
36. Rowan SJ, Stoddart JF (1999) *Org Lett* 1:1913–1916.
37. Glink PT, Oliva AI, Stoddart JF, White AJP, Williams DJ (2001) *Angew Chem Int Ed* 40:1870–1875.
38. Fujita M (1998) *Chem Soc Rev* 27:417–425.
39. Leininger S, Olenyuk B, Stang P (2000) *J Chem Rev* 100:853–908.
40. McKinlay RM, Cave GWV, Atwood JL (2005) *Proc Natl Acad Sci USA* 102:5944–5948.
41. Elliott EL, Hernandez GA, Linden A, Siegel JS (2005) *Org Biomol Chem* 3:407–413.
42. Iwasawa T, Hooley RJ, Rebek J, Jr (2007) *Science* 317:493–496.